

WAVE ATTENUATION BY THE DELTAPORT  
FLOATING BREAKWATER

CENTRE FOR NEWFOUNDLAND STUDIES

**TOTAL OF 10 PAGES ONLY  
MAY BE XEROXED**

(Without Author's Permission)

RICHARD D. YETMAN







WAVE ATTENUATION BY THE DELTAPORT FLOATING BREAKWATER

by

© Richard D. Yetman, B.Eng.

A thesis submitted to the School of Graduate  
Studies in partial fulfillment of the  
requirements for the degree of  
Master of Engineering

Faculty of Engineering and Applied Science  
Memorial University of Newfoundland

April 1988

St. John's

Newfoundland

Canada

Permission has been granted to the National Library of Canada to microfilm this thesis and to lend or sell copies of the film.

The author (copyright owner) has reserved other publication rights, and neither the thesis nor extensive extracts from it may be printed or otherwise reproduced without his/her written permission.

L'autorisation a été accordée à la Bibliothèque nationale du Canada de microfilmer cette thèse et de prêter ou de vendre des exemplaires du film.

L'auteur (titulaire du droit d'auteur) se réserve les autres droits de publication; ni la thèse ni de longs extraits de celle-ci ne doivent être imprimés ou autrement reproduits sans son autorisation écrite.

ISBN 0-315-50478-1

To the memory of my  
Grandmother and dear friend  
Mrs. B. L. Yetman (1911-1987)

ABSTRACT

Deltaport is basically a large floating breakwater intended for use in the Hibernia region. This thesis describes an exploratory investigation into its wave attenuation characteristics. The breakwater portion of its structure is porous like and consists of a staggered array of tubes. When wave energy impinges on such a structure, some of it is reflected back, some is transmitted through, under and around the structure, and the rest is dissipated. Initially, we had hoped to completely isolate the contributions to this energy balance. However, because of the complex nature of the Deltaport Structure, we found this goal to be extremely difficult, if not impossible, to attain. To simplify, we decided to consider only two dimensional sections of the structure and concentrate on the effect of porosity. A two dimensional section of the breakwater structure was installed in the wave tank at Memorial University of Newfoundland, and its attenuation characteristics for several levels of porosity were measured. As expected, it was found that porosity greatly reduces attenuation.

Two theoretical procedures were developed for the two dimensional setup. One, known as Dean's method, assumes the structure to be a nonporous vertical thin plate and is based on a potential flow description of the water motion.

It gives very simple expressions for reflection and transmission and allows one to get a rough but quick look at performance. The other procedure is basically a finite difference numerical simulation based on the Navier-Stokes equations. It allows for wave energy dissipation, something not considered in a potential flow formulation. It also has a feature by which the porous nature of the structure can be accounted for. We believe we are the first to use this in a study of breakwater performance. Comparisons of the latter with the experiment show reasonable agreement.

Numerical schemes are available that can handle three dimensional bodies interacting with waves; however, they can only deal with nonporous structures. One of these schemes, known as the Panel Method, accounts for wave diffraction and is based on a distribution of potential flow singularities over the wetted surface of the body. This technique was also applied to the Deltaport geometry. Obviously, because it ignores porosity, it represents an ideal. The two dimensional setup suggests that it overpredicts attenuation.

The report also gives some suggestions for future work. For example, it might be possible to develop correction factors for the Panel Method based on the two dimensional setup.

ACKNOWLEDGEMENTS

Many people at Memorial University contributed significantly to the writing of this thesis, and to them I extend my very sincere thanks. First, I would like to thank my supervisors, Dr. M.J. Hinchey and Professor H. L. Snyder, for their guidance and support. My thanks are also due to Dr. G.R. Peters, Dean of Engineering, Dr. T. R. Chari, Associate Dean of Engineering, and Dr. D. B. Muggeridge, Chairman, Ocean Engineering Research Group, not only for their personal encouragement but also for their strong support of the program.

My tenure here at Memorial was made possible through the financial support provided through the efforts of Professor H.L. Snyder and Mr. T.W. Kierans, for these efforts I am grateful. I should also like to thank the MUN wave tank crew and fellow graduate students, Mrs. P.M. Dunphy and Mr. G.L. Rzentkowski for their valuable suggestions and helpful discussions.

Special thanks are extended to Mr. D. Sen for countless hours of help and guidance; his interest and support of my work are responsible for much of what I have learned as a graduate student.

I should like to thank Mrs. M. Crocker whose care and patience in typing this work was considerable and is very much appreciated.

Finally, I thank my mother and father who have been the inspiration for and are still the guiding force behind all that I do, including this thesis.

TABLE OF CONTENTS

	Page
ABSTRACT	i
ACKNOWLEDGEMENTS	iv
TABLE OF CONTENTS	vi
LIST OF TABLES.	ix
LIST OF FIGURES	x
NOMENCLATURE	xii
CHAPTER I INTRODUCTION	1
1.1 Background on Breakwaters	1
1.2 The Deltaport Concept	6
1.3 Objective of Present Work.	10
1.4 Some Modelling Considerations	12
CHAPTER II HYDRODYNAMIC BACKGROUND	13
2.1 Governing Equations for Small Amplitude Waves	13
2.2 Wave Characteristics	17
2.2.1 Phase Speed	17
2.2.2 Group Speed	18
2.2.3 Wave Energy Flux	19
2.3 Wave Attenuation Mechanisms	20
2.3.1 Reflection	21
2.3.2 Dissipation	21

	Page
CHAPTER III THEORETICAL FORMULATIONS	22
3.1 Dean's Method	22
3.2 The SOLA-VOF Method	26
3.3 The Panel Method	32
CHAPTER IV EXPERIMENTAL PROGRAM	38
4.1 Wave Tank Facility	38
4.2 Model Construction	38
4.3 Physical Barriers	44
4.4 Model Waves	45
4.5 Data Acquisition	46
4.6 Scale Considerations	49
CHAPTER V RESULTS	52
5.1 Dean's Method	52
5.2 The SOLA-VOF Method	52
5.2.1 Viscosity Effects	55
5.2.2 Surface Tension Effects	57
5.2.3 Effect of Grid Size	58
5.3 Comparisons of SOLA-VOF and Dean's Method	58
5.4 The Panel Method	59
5.5 Experiment	70
5.5.1 Thin Plate Case	70
5.5.2 Rectangular Barrier Case	70
5.6 Comparisons of SOLA-VOF and the Thin Plate Experiments	73

CHAPTER VI CONCLUSIONS AND SUGGESTIONS FOR  
REFERENCES FUTURE WORK

LIST OF TABLES

Table		Page
1.1	Deltaport Basic Information	8
3.1	Panel Method Discretization	35
5.1	SOLA-VOF: Viscosity Effects	56
5.2	SOLA-VOF: Surface Tension Effects	57
5.3	Panel Method Results	60
5.4	Panel Method/Shore Protection Manual Comparison	69

LIST OF FIGURES

Figure	Title	Page
1.1	Various Breakwater Designs	2
1.2	Artist's Conception of the Deltaport Concept	7
2.1	Wave Train and Coordinate Axis	14
3.1	Vertical Barrier Setup	24
3.2	Relationship Between R, T & $\lambda$	25
3.3	Wave Tank Simulation	29
3.4	Typical Output from SOLA-VOF Method	31
3.5	Panel Method Position Markers	36
4.1	Wave Tank Facility	39
4.2	Model Construction Drawings and Pictures	41
4.3	Barrier Geometries	43
4.4	$R_e$ vs $C_D$	51
5.1	Reflection vs Barrier Depth: Dean's Method	53
5.2	Transmission vs Barrier Depth: Dean's Method	53
5.3	Reflection vs Barrier Depth: SOLA-VOF	54
5.4	Transmission vs Barrier Depth: SOLA-VOF	54
5.5	Dean's Method vs SOLA-VOF: 0.8 Hz	61
5.6	Dean's Method vs SOLA-VOF: 0.9 Hz	62
5.7	Dean's Method vs SOLA-VOF: 1.0 Hz	63
5.8	Dean's Method vs SOLA-VOF: 1.1 Hz	64
5.9	Dean's Method vs SOLA-VOF: 1.2 Hz	65
5.10	Diffraction Pattern for Semi-Infinite Barrier	68

(Source: Shore Protection Manual)

5.11	Experimental Data: Solid Thin Plate	71
5.12	Experimental Data: Porous Thin Plate	71
5.13	Experimental Data: Solid Rectangular Barrier	72
5.14	Experimental Data: Porous Rectangular Barrier	72
5.15	Experimental/SOLA-VOF Comparison	74
5.16	Porous Barrier Geometry: SOLA-VOF	75

NOMENCLATURE

A	amplitude
a	unit complex wave amplitude
$C_D$	drag coefficient
$C_g$	group speed
C	celerity
c	sound speed
D	barrier depth
d	water depth
E	energy
F	fluid configuration
G	Green's function for complex source
g	acceleration due to gravity
H	wave height
$I_1$	modified Bessel function
K	diffraction parameter
$K_1$	modified Bessel function
KE	kinetic energy
k	wave number
$N_{KC}$	Keulegan-Carpenter number
PE	potential energy
P	pressure
R	reflection coefficient
$R_e$	Reynolds number

T	transmission coefficient
$T_p$	wave period
t	time
u	velocity in x-direction
V	flow speed
v	velocity in y - direction
x	horizontal direction
y	vertical direction
$\eta$	free surface elevation
$\lambda$	wave length
$\rho$	density of water
$\sigma$	strength of complex source
$\phi$	velocity potential
$\omega$	angular frequency

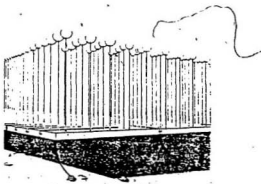
## INTRODUCTION

1.1 Background on Breakwaters

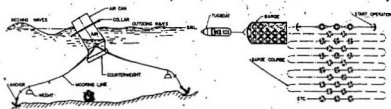
Heavy seas have always caused problems for coastal areas and offshore structures. In some cases, these problems have been alleviated over the years by the use of wave attenuating breakwaters. Breakwaters have been categorized under the two general headings of "floating" and "non-floating". Non-floating or fixed breakwaters provide the best attenuation because a fixed solid wall can reflect or dissipate almost all of the incident wave energy, thereby permitting little or no transmitted wave past the breakwater. However, their cost goes up significantly with increasing water depth.

The versatility, mobility, and relatively lower cost of a floating breakwater makes it a viable option in many cases. Over the years, many different ideas and designs have been constructed and tested [1 to 9]. Some of these designs have had very good success and some have been total failures. Most have some degree of porosity. This cuts down reflection and makes the sea-state in front more desirable.

Figure 1.1 shows two of these designs. The first, a Tethered Float Breakwater, is constructed of a large number of very buoyant floats with a characteristic



TETHERED FLOAT BREAKWATER



BOWLEY WAVE BARRIER

Figure 1.1 Various Breakwater Designs

dimension about equal to the wave height. They are independently tethered below the surface in a water depth many times the float diameter. The floats are driven in opposition to the waves by the pressure gradient field and the dominant attenuation mechanism is drag from the resultant buoy motion. Potential applications include harbour and marina protection as well as for offshore terminals. It has also been suggested for use as a low cost and flexible beach erosion control system.

The second system shown is the Bowley Wave Barrier which was developed by Professor W.W. Bowley of the University of Connecticut. This system consists of an array of fendered cylindrical canisters which due to their buoyancy oscillate in wave action. This induced motion creates a secondary wave pattern emanating from the canister itself. Theory suggests that it is this secondary wave which superimposes with the incident wave to create wave toppling and thus an overall reduction in wave height beyond the array.

A review of the literature on floating breakwaters indicates that, to date, the vast majority of floating breakwater analyses have been very qualitative. Prototype and model testing have been the only real reliable way of judging their performance. In a November 1986 Conference held under the auspices of the Coastal Engineering Research

Council of the American Society of Civil Engineers (ASCE), a paper was presented by Murakami et al. [7] which stated "Since Jarlan (1961) proposed the perforated vertical wall breakwater, many different kinds of permeable wall breakwaters have been designed. The hydraulic characteristics of these breakwaters have been examined experimentally for the most part. The theoretical solutions for the reflection and the transmission coefficients have been obtained only for the breakwaters with a comparatively simple cross section geometry".

Attempts have been made to include porosity into the theoretical treatment of breakwaters. One two dimensional approach, developed by Madsen [8], is based on a quasi-steady hydraulic resistance model for the structure. The flow within the structure causes energy dissipation. For long waves, this would show up as a difference in water level across the structure. For steady state flows through the structure, this difference can be measured in a flume. Integration over a wave cycle could use this to get the energy dissipated within the structure during each cycle and one could calculate an average power dissipation. The quasi-steady assumption means that the resistance approach is probably only good for long waves.

Another two-dimensional approach was developed by Finnigan and Yamamoto [9]. They assumed the flow within the

structure to be due to a balance of viscous and pressure forces only. This is the well known porous-plug or Darcy flow model. Unfortunately, it ignores turbulence, which could be the major source of dissipation in the Deltaport structure, which is the breakwater being considered herein.

Neither of the above approaches was used in the present work. Instead, a transient finite difference scheme based on the Navier-Stokes equations was employed. We believe we are the first to make use of this in a breakwater context. With a sufficiently refined grid, it should be able to accurately model turbulent flow within the structure. Unfortunately, with a refined grid, the scheme is computationally very expensive. Engineers are usually not interested in the details of eddy motions within a turbulent flow. Usually, the diffusive or macroscopic character of the eddy motions is of greater interest, because this is responsible for energy dissipation. Models have been developed which avoid consideration of the details of eddy motion [10]. They are known as eddy viscosity models, and they are based on a time averaging of the Navier-Stokes equations. When added to numerical schemes, much coarser and thus computationally less expensive grids can be used. Unfortunately, it is beyond the scope of the present work to add such to the basic code employed. So, we were forced to use as refined a grid as possible.

As time progresses, the need for accurate solutions to breakwater problems becomes increasingly important. This thesis addresses the possibility of using recent advancements in technology, both in theory and computer speed, to obtain analytic solutions to floating breakwater problems.

### 1.2 The Deltaport Concept

The quest for hydrocarbon resources has forced exploration far out into the oceans at distances never before considered feasible. At these ever increasing distances, the danger, inefficiency, and cost of recovering the natural resource all increase. Clusters of drill rigs and production platforms in these areas require frequent service and supplies of men and materials. The danger to personnel and the cost of service and supply have prompted research on and development of an offshore support base known as Deltaport (Figure 1.2 and Table 1.1). Research into this concept started in 1983 at Memorial University of Newfoundland and is still ongoing. To date, there has been no indepth design done on the structure itself, and it should be noted that the idea is still very much at a conceptual level. The design parameters, which are outlined in this section, are very descriptive in nature and research is now being performed into how best to incorporate these

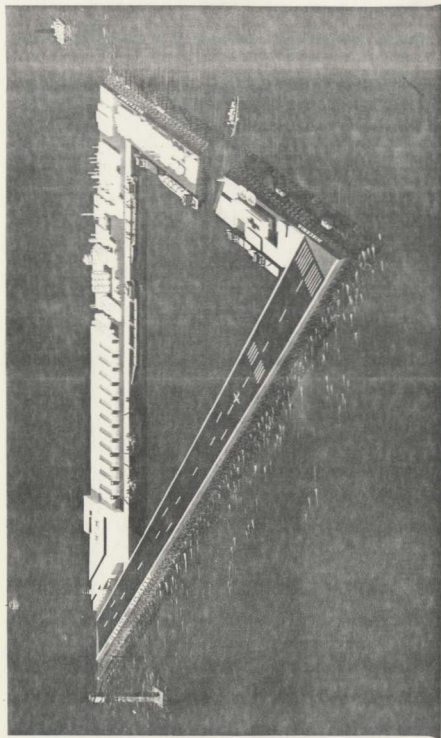


Figure 1.2 Artist's Conception of the Deltaport Concept

DELTAPORT CHARACTERISTICS

L.O.A.	600-1000 m
Dry Weight	1200-1800 M.T.
Draft (Range)	20-40 m
Free Board (Range)	40-20 m
Beam (Per Side)	90-100 m
Depth	60 m
Shape	Equilateral Triangle

SITE CONDITIONS - HIBERNIA - IN SITU

Wave	
Maximum (100-year)	30.5 m, 16.0 sec.
Significant (Normal)	5.0 m, 8.6 sec.
Astronomical Tide	1.2 m
Water Depth	50.0 m
Current	
Surface	0.7 m/s - 1.1 m/s
Mid-Depth	0.4 m/s - 0.6 m/s
Bottom	0.2 m/s - 0.4 m/s

TABLE 1.1 - DELTAPORT BASIC INFORMATION

into one comprehensive structure. Figure 1.2, which is an artists conception of the prototype, reflects relatively accurately the intent and general configuration of the Deltaport concept. Also, Table 1.1 gives as detailed a description as is now available on the dimensions and operating conditions of the Deltaport, as well as a summary of the environmental conditions it is to operate in.

Deltaport, named for its triangular configuration, is being designed for free rotation about a single point mooring and will be able to move under its own power to avoid ice fields and icebergs. Its structure will be made up of thousands of interconnected buoyancy units, and its maintenance will be carried out continuously while on site. This man-made floating island will have features to increase safety and cost effectiveness. It will have a short take off and landing (STOL) air strip to accommodate appropriate fixed wing aircraft. There will be on board facilities for liquefaction of natural gas, crude oil refinement, diesel power generation, subsea completion, and on board oil storage. Medical services, living accommodation and administration facilities will also be incorporated into the design of the Deltaport concept.

An important feature of the Deltaport concept, which has particular relevance to this thesis work, is the sheltered harbour or breakwater effect. Due to the immense

size of the structure (nearly one square kilometre), it has great potential for the attenuation of wave energy and this will allow it to provide a sheltered lee in the midst of a harsh North Atlantic ocean environment. For the analysis of the structure as a breakwater, assumptions have to be made as to its internal configuration. A configuration used in earlier tests [11,12] on a 1:50 scale model was selected to serve as the geometry used herein. This is defined in later sections.

The total cost of a Deltaport is expected to be in the range of three to four billion dollars [11]. The anticipated cost savings over its seventy-five year life is in the range of sixty billion dollars [11]. These savings are expected to come from reduced transportation and service costs, production of marginally economic fields, and the liquefaction and production of natural gas.

Tragic accidents have shown that the offshore environment is relentless and unforgiving. Deltaport would provide close-by refuge for the industry as well as a base for medical and safety operations. The increased use of fixed-wing aircraft and the environmental shelter provided to marine vessels would reduce risks immensely.

### 1.3. Objective of Present Work

Any structure which sits in an ocean environment

and causes an interference to wave propagation could be considered in some capacity a breakwater. The Deltaport concept is no exception to this rule. In fact, one of the most important functional features of the concept will be its capacity to attenuate wave energy. At present, the technology for analyzing breakwater performance is not at a very advanced stage. To date, the design process has generally been qualitative, with the ability to attenuate wave energy measured only after the prototype is in operation. With the Deltaport capital costs being so high and the time invested so intense, it is not acceptable to leave its final performance to these elements of chance.

When wave energy impinges on a structure such as Deltaport, some of it is reflected, some is transmitted, and the rest is dissipated. The goal of the project was to isolate these energy components. This is an extremely difficult, if not impossible, thing to do analytically for a porous three dimensional structure. Because of this, a two dimensional section of the Deltaport structure was isolated for study.

A model of this was installed in the wave tank at Memorial University of Newfoundland, and its attenuation characteristics for several levels of porosity were measured. Two theoretical models were developed for the two dimensional setup. One is based on potential flow while the

other is based on the Navier-Stokes equations. Comparisons with the experiment were promising. Numerical schemes are available which can handle the interaction of three dimensional non-porous bodies with waves. One of these is known as the Panel Method for wave diffraction and this was also applied to the Deltaport geometry.

#### 1.4 Some Modelling Considerations )

In order to create physical and numerical models of floating breakwaters which can approximate the response of the Deltaport concept, certain assumptions and simplifications were made.

Deltaport while in operation would be securely moored at one of its pivot points. The relatively large body size compared to the wave profile should produce very small body motions. Previous test work [12] on scale models has confirmed this fact. Because of this, the amount of wave energy produced by the body motions would be very small. The time period of the body motions has also been shown to be much greater [12] than the incident wave period. Given these facts, it was decided to view Deltaport as a fixed structure. Treating Deltaport as fixed not only accurately reflects the prototype in operation, but it also simplifies the analytical and physical modelling techniques.

## CHAPTER II

## HYDRODYNAMIC BACKGROUND

2.1 Governing Equations for Small Amplitude Waves

It is assumed that waves travel progressively in the x-direction in the x-y plane. It is also assumed that the water surface is uncontaminated with no underlying current and that the wave maintains a permanent form over a smooth horizontal bed. Water is also taken to be incompressible and inviscid, and the flow is taken to be irrotational. The water depth  $d$  is constant. Figure 2.1 shows the general form of the wave train.

In this schematic, the wave height (from crest to trough) is taken to be  $H$ , the wave length is shown as  $\lambda$  and  $T_p$  is the wave period. The wave speed, or celerity, can be defined as  $C$ , where:

$$C = \lambda/T_p \quad (2.1)$$

It is also convenient to show angular frequency  $\omega$  as:

$$\omega = 2\pi/T_p \quad (2.2)$$

and the wave number  $k$  as:

$$k = 2\pi/\lambda \quad (2.3)$$

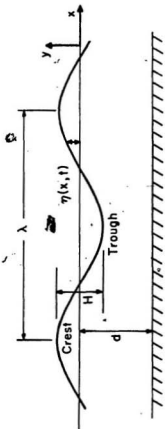


Figure 2.1 Wave Train and Coordinate Axis

A velocity potential  $\phi$  is needed which satisfies the Laplace equation:

$$\nabla^2 \phi = 0 \quad (2.4)$$

For a two dimensional wave form in  $x$  and  $y$ , this reduces to:

$$\frac{\partial^2 \phi}{\partial x^2} + \frac{\partial^2 \phi}{\partial y^2} = 0 \quad (2.5)$$

The velocity potential is subject to the following boundary conditions:

$$\frac{\partial \phi}{\partial y} = 0 \quad \text{at } y = -d \quad (2.6)$$

$$\frac{\partial \eta}{\partial t} + \frac{\partial \phi}{\partial x} \frac{\partial \eta}{\partial x} - \frac{\partial \phi}{\partial y} = 0 \quad \text{at } y = \eta \quad (2.7)$$

$$\frac{\partial \phi}{\partial t} + \frac{1}{2} \left[ \left( \frac{\partial \phi}{\partial x} \right)^2 + \left( \frac{\partial \phi}{\partial y} \right)^2 \right] + g\eta = f(t) \quad \text{at } y = \eta \quad (2.8)$$

where  $\eta$  is the free surface elevation about the still water line and  $g$  is the acceleration due to gravity.

Equation (2.6) corresponds to the bottom boundary condition which says that the vertical particle velocity there is zero. Equation (2.7) is the surface kinematic boundary condition which says that the velocity of the fluid particle normal to the free surface is equal to the velocity of the free surface itself. The surface dynamic boundary condition, given by equation (2.8), states that the pressure at the surface, given by the unsteady Bernoulli equation, is

constant, assuming of course that atmospheric pressure is constant and that surface tension is zero.

Small amplitude wave theory, sometimes known as Airy wave theory, was developed because of two serious difficulties encountered in attempts to obtain an exact solution for a two-dimensional wave train. The first is that the free surface boundary conditions are non-linear and the second is that these conditions are defined to be at the free surface which is initially unknown. As its name implies, small amplitude wave theory assumes the wave height to be much smaller than both the wave length and the still water depth [13,14]. This assumption makes the nonlinear terms in the surface boundary conditions, equations (2.7) and (2.8), negligible in comparison to the linear terms. Thus, these equations reduce to:

$$\frac{\partial \phi}{\partial y} - \frac{\partial \eta}{\partial t} = 0 \quad \text{at } y = 0 \quad (2.9)$$

$$\frac{\partial \phi}{\partial t} + g\eta = 0 \quad \text{at } y = 0 \quad (2.10)$$

The separation of variables procedure can be used to find a solution which satisfies Laplace's equation and the various constraints. It gives

$$\phi = \frac{gH}{2kC} \frac{\cosh k(y+d)}{\cosh(kd)} \sin k(x-Ct) \quad (2.11)$$

$$\eta = \frac{H}{2} \cos k(x - Ct) \quad (2.12)$$

Substitution of these equations back into the free surface conditions gives the dispersion relationships:

$$\omega^2 = gk \tanh(kd) \quad (2.13)$$

$$C^2 = \frac{g}{k} \tanh(kd) \quad (2.14)$$

## 2.2 Wave Characteristics

### 2.2.1 Phase Speed

The phase speed for a linearized wave can be obtained from equation (2.14):

$$C^2 = \frac{g}{k} \tanh(kd) \quad (2.14)$$

When deep water waves are considered, the term  $kd$  approaches infinity and

$$\tanh(kd) = 1 \quad (2.15)$$

Thus, for deep water, the dispersion relationship reduces to:

$$C^2 = \frac{g}{k} = \frac{g\lambda}{2\pi} \quad (2.16)$$

This means that deep water waves are dispersive. Because  $C$  is a function of  $\lambda$ , the components of a storm generated deep water wave system tend to separate from one another, with

the longer waves leaving the shorter ones behind. When the shallow water case is studied, the  $\tanh(kd)$  term in equation 2.14 reduces to:

$$\tanh(kd) \approx kd \quad (2.17)$$

In this case, the dispersion relationship reduces to :

$$C^2 = \frac{g}{k} (kd) = gd \quad (2.18)$$

This shows that shallow water waves are non-dispersive because  $C$  is not a function of  $\lambda$

### 2.2.2 Group Speed

When sinusoidal waves within a narrow band of frequencies are superimposed, an envelope is generated which travels at a speed called the group speed, denoted by  $C_g$ . The phase speed of an individual wave within the envelope is given by [14]:

$$C = \frac{\omega}{k} \quad (2.19)$$

The speed of the envelope itself is [14]:

$$C_g = \frac{d\omega}{dk} \quad (2.20)$$

For deep water, the frequency can be written as [14]:

$$\omega^2 = kg \quad (2.21)$$

If frequency is differentiated with respect to wave number, the following relationship is obtained:

$$2\omega \frac{d\omega}{dk} = g \quad (2.22)$$

Substituting equation (2.22) into equation (2.20) yields the relationship:

$$C_g = \frac{d\omega}{dk} = \frac{g}{2\omega} = \frac{1}{2} C \quad (2.23)$$

Therefore, it is shown that, for deep water, the phase speed is twice the group speed. For shallow water, the frequency can be written as [14]:

$$\omega^2 = k^2 g d \quad (2.24)$$

Differentiating equation (2.24) yields:

$$2\omega \frac{d\omega}{dk} = 2kgd \quad (2.25)$$

Substituting equation (2.25) into equation (2.20) yields:

$$C_g = \frac{d\omega}{dk} = \frac{2kgd}{2\omega} = \frac{gd}{C} \quad (2.26)$$

Equation (2.18) shows that the phase speed for shallow water is equal to  $\sqrt{gd}$ . Substitution of this into equation (2.26) gives:

$$C_g = \frac{gd}{\sqrt{gd}} = \sqrt{gd} \quad (2.27)$$

Thus, the group speed is equal to the phase speed.

### 2.2.3 Wave Energy Flux

The total energy in a unit column of water is the sum of the kinetic and potential energies. These energies are equal [14] and are given by:

$$PE = KE = \frac{1}{4} \rho g A^2 = \frac{1}{16} \rho g H^2 \quad (2.28)$$

where A is the wave amplitude; H is the wave height and  $\rho$  is the water density. Therefore, the total energy in the water column is given by:

$$E = KE + PE = \frac{1}{2} \rho g A^2 = \frac{1}{8} \rho g H^2 \quad (2.29)$$

If a vertical cross section of unit width perpendicular to the direction of wave propagation is considered, the rate at which energy crosses this is given by [14]:

$$\text{Energy Flux} = C_g E = C_g \frac{1}{2} \rho g A^2 = C_g \frac{1}{8} \rho g H^2 \quad (2.30)$$

### 2.3 Wave Attenuation Mechanisms

When looking at the wave attenuating mechanisms of floating breakwaters, the relationship between wave height and wave energy must be considered. It can be seen from equation (2.29) that the wave energy is directly proportional to the square of the wave amplitude (or wave height). In other words

$$E \propto A^2 \quad E \propto H^2 \quad (2.31)$$

Considering this, anything which redirects energy or takes energy away from the wave will reduce the height of the wave. This is, of course, the desired effect. It should be noted that the other terms of equation (2.29) are constant and the only variable relationship is between A or H and E.

The designer of a floating breakwater has control over its size, shape, depth below the water line, orientation, rigidity and porosity. These physical characteristics influence the effectiveness of its wave attenuation properties: two of the major ones being reflection and dissipation.

### 2.3.1 Reflection

When an incident wave encounters an obstruction, some of its energy is directed back into the wave field. The amount of reflected energy reduces the total energy available on the lee side of the obstruction. Therefore, the ability of a breakwater to reflect energy is very important in determining its overall efficiency. Reflection is thought to be the most important factor when considering the design of a floating breakwater [1 to 9]. It can lead to very confused seas in front of the structure.

### 2.3.2 Dissipation

When an incident wave interacts with a floating structure, some of its energy is dissipated. The loss of this energy also contributes to a reduction of wave height on the lee side of the structure. For porous structures, water turbulence, set up by the flow through the structure, is the major source of dissipation [13,14,15]. The latter was talked about briefly earlier.

## CHAPTER III

## THEORETICAL FORMULATIONS

At the present time, there are no analytical or numerical procedures available for treating the interaction of waves with complex, three dimensional, porous-like structures such as Deltaport. However, for non-porous structures, some procedures have been reported. One of these is known as the Panel Method for wave diffraction, and this is applied herein to Deltaport. Obviously, because it ignores porosity, its predictions require careful scrutiny. Also, the scheme is based on potential flow concepts. In other words, it ignores viscosity.

A finite difference scheme is available that can handle viscosity and porosity. It is based on the Navier-Stokes equations. Unfortunately, it is computationally very expensive, and because of this, it is restricted to two dimensional geometries. It is used below to study a two dimensional section of the Deltaport structure. Another much simpler two dimensional model is also applied to the structure.

### 3.1 Dean's Method

Dean's method is perhaps the simplest of the three methods to be studied. This method assumes the water to be

deep and its motion to be two dimensional. It also assumes that the barrier is a rigid nonporous vertical thin plate.

Figure 3.1 shows a schematic of the set up for which Dean's method is applicable.

Using potential flow concepts, Dean [16,17] developed equations for the reflection and transmission coefficients of this configuration. These equations are:

$$R = \frac{\pi I_1}{\sqrt{\pi^2 I_1^2 + K_1^2}} \quad (3.1)$$

$$T = \frac{K_1}{\sqrt{\pi^2 I_1^2 + K_1^2}} \quad (3.2)$$

where R is the reflection coefficient, T is the transmission coefficient, and  $I_1$  and  $K_1$  are modified Bessel functions with argument  $kD$ . These relationships are shown graphically in Figure 3.2. They give a rough but quick look at breakwater performance.

Note that for  $2\pi D/\lambda$  greater than 2 the reflection coefficient R is practically one and the transmission coefficient T is near zero. This is not surprising because water motion falls off exponentially as one moves down from the water surface. The fall off is given by

$$e^{-\frac{2\pi y}{\lambda}} \quad (3.3)$$

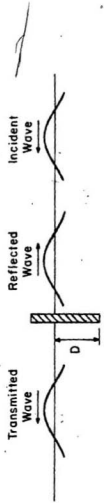


Figure 3.1 Vertical Barrier Setup

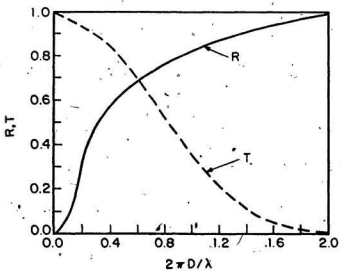


Figure 3.2 Relationship Between R, T &  $\lambda$

So, at  $y = -D$  for the case in question, there is very little water motion and thus very little transmission. Once the reflection and transmission coefficients are known, the wave heights can be calculated as follows:

$$H_R = R * H_I \quad (3.4)$$

$$H_T = T * H_I \quad (3.5)$$

where  $H_I$  is the incident wave height.

### 3.2 The SOLA-VOF Method

The term SOLA-VOF [18] is an acronym derived in two sections, VOF meaning volume of fluid, and SOLA meaning solution algorithm. This method was developed to solve transient fluid flow problems with multiple free boundaries. The SOLA-VOF method basically divides a region of fluid up into a large number of finite difference cells. The accuracy of the SOLA-VOF method is determined greatly by the size of the cells and the time step,  $\delta t$ , used to march the solution forward step by step in time.

Basically, there are three steps involved in advancing a solution through one increment,  $\delta t$ , in time.

- 1) Explicit approximations of the Navier-Stokes equations

$$\frac{\partial u}{\partial t} + u \frac{\partial u}{\partial x} + v \frac{\partial u}{\partial y} = -\frac{1}{\rho} \frac{\partial p}{\partial x} + \nu \left( \frac{\partial^2 u}{\partial x^2} + \frac{\partial^2 u}{\partial y^2} \right) \quad (3.6)$$

$$\frac{\partial v}{\partial t} + u \frac{\partial v}{\partial x} + v \frac{\partial v}{\partial y} = -\frac{1}{\rho} \frac{\partial p}{\partial y} + \nu \left( \frac{\partial^2 v}{\partial x^2} + \frac{\partial^2 v}{\partial y^2} \right) \quad (3.7)$$

are used to compute updated velocities  $u$  and  $v$  on cell boundaries using previous time level values for all advective, pressure and viscous accelerations.

2) To satisfy the continuity equation given by

$$\frac{\partial p}{\rho c^2} + \frac{\partial u}{\partial x} + \frac{\partial v}{\partial y} = 0 \quad (3.8)$$

pressures  $p$  are iteratively adjusted in each cell and the velocities resultant from these pressure changes are added to the velocities generated in step one. The iteration is needed because pressure changes in one cell affect the four surrounding cells.

3) Finally, a function called the  $F$  function governed by the equation

$$\frac{\partial F}{\partial t} + u \frac{\partial F}{\partial x} + v \frac{\partial F}{\partial y} = 0 \quad (3.9)$$

which defines the fluid regions must be updated to give the new fluid configuration. If the value of  $F$  equals 1, then the cell is completely filled with fluid; if  $F$  equals 0, the

cell contains no fluid; and if the value of  $F$  is between 0 and 1, then the cell contains the free surface.

Complete details of the SOLA-VOF method can be found in Nichols et al [18].

For the present work, the SOLA-VOF computer program was modified to simulate the wave tank set up. For this, an oscillating flap type wave board was used to generate the incident waves. Barriers were introduced into the simulation by blocking out cells in the mesh.

Figure 3.3 shows the wave tank configuration as it was input into the computer simulation.

For execution of the SOLA-VOF program, the VAX/VMS 8800 computer system at Memorial University was used. It was originally planned to scale the exact dimensions of the Memorial University wave tank, but this was found to be computationally expensive. Because of this, the working length of the tank was shortened to 18 m, with the barrier placed 11 m from the wave board. We believe that these dimensions are adequate for the development of an approximately steady state reflected wave envelope and transmitted wave together with the basically undisturbed incident wave. The working height of the tank was set at 1.5 m, and the water depth was set at 0.9 m. The beach used in the simulation is basically a vertical wall. The run time for each simulation was chosen, using group speed

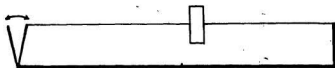
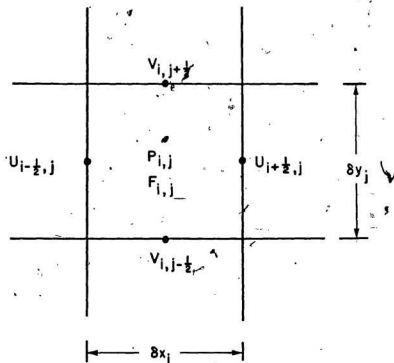


Figure 3.3 Wave Tank Simulation

concepts, such that the transmitted wave did not get contaminated by reflection from the wall. This also allowed adequate time for a wave envelope to form between the barrier and the wave board. Figure 3.4, which is typical output from the program, clearly shows the envelope. The figure is basically a plot of the maximum and minimum surface elevations which occurred, at specific locations along the tank, during the run.

Region 1 is the area where the incident wave is basically unaffected by the reflected wave. In this region, maximum and minimum surface elevations are a measure of the incident wave height  $H_I$ . The minor fluctuations in this region could be a result of start up transients developed in the program. They could also be a parasitic wave phenomenon set up by the flap generator [14].

Region 2 is the area where the reflected wave is superimposing with the incident wave to create a wave envelope. As mentioned previously, the reflection coefficient can be determined from the equation:

$$R = \frac{H_{\max} - H_{\min}}{H_{\max} + H_{\min}} \quad (3.10)$$

where  $H_{\max}$  is the maximum height of the envelope and  $H_{\min}$  is the minimum height.

Region 3 is the area behind the barrier where the transmitted wave height  $H_T$  can be calculated in the same way

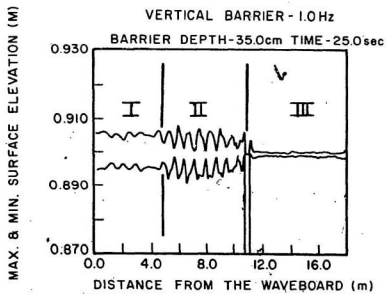


Figure 3.4. Typical Output from SOLA-VOP Method

as the incident wave height in Region 1. The transmission coefficient  $T$  can then be determined very easily from the following equation:

$$T = H_T/H_I \quad (3.11)$$

Assuming there are no energy losses and that the numerical method is 100% accurate with no accumulated computational error, then the relationship

$$R^2 + T^2 = 1 \quad (3.12)$$

should hold true, if the waves are steady and there are no parasitic phenomena.

Normally, the simulation used a total of 250 divisions along the horizontal (18m) axis and 30 divisions along the vertical (1.5m) axis. In other words, there were usually 7500 finite difference cells.

### 3.3 The Panel Method

When a large body is inserted into a wave field, it scatters the waves. For small amplitude waves, this scattering or diffraction problem is linear, and for a nonporous body, the total potential at any point in the flow field can be written as:

$$\phi = \phi_I + \phi_D \quad (3.13)$$

where  $\phi_I$  is the incident wave potential and  $\phi_D$  is the potential of the scattered waves.

According to the singularity distribution procedure, the latter can be represented as a distribution of singularities over wetted surface of the body  $S_w$ . For complex source type singularities, this distribution is [13,14]:

$$\phi_D(P) = \frac{1}{4\pi} \int_{S_w} \sigma(Q) G(P,Q) dS \quad (3.14)$$

where  $\sigma$  is the complex source strength,  $G$  is the complex source singularity, and  $P$  and  $Q$  are points on  $S_w$ .

Substitution of the expressions for  $\phi_I$  and  $\phi_D$  into the body boundary condition:

$$\frac{\partial \phi}{\partial n} = 0 = \frac{\partial \phi_D}{\partial n} + \frac{\partial \phi_I}{\partial n} \quad (3.15)$$

gives an equation for  $\sigma$ . In theory, the strength distribution can be adjusted so that this boundary condition is satisfied at every point on the wetted surface. For complex shapes, the proper distribution of  $\sigma$  is difficult to find analytically, and an approximate solution is usually sought instead.

The Panel Method gives such a solution. It divides the wetted surface into a finite number of panels and looks for the value of  $\sigma$  at the centroid of each panel. These are adjusted so that the body boundary condition is satisfied at each centroid. The procedure gives a system of algebraic equations for the  $\sigma$ 's at the centroids.

Sen [19] developed a computer program based on these ideas. In its basic form, it gives pressures and thus loads acting on body surfaces. For the present work, it was modified so that it gave the water surface profile near the body. These modifications were quite extensive and took quite some time to implement. Special care had to be taken to avoid numerical stability problems which are often inherent in such codes. A subroutine was also added which automatically created the triangular Deltaport shape and generated the panel geometry. This made changing the panel geometry straight forward.

For execution of the Panel Method program, the VAX/VMS 8800 computer system at Memorial University was used. This system placed constraints on the program such as space allocation and the amount of precision in the program calculations. Within the main program, an  $N \times N$  complex number matrix has to be inverted,  $N$  being the number of geometric panels. As the number of panels got very large, this inversion for the lower range of wave lengths would

break down due to problems resulting from double precision numbers not being sufficiently accurate, and although the computer system could handle quadruple precision of real numbers, it couldn't handle this for complex numbers. Table 3.1 shows, for several wavelengths, the number of panels beyond which the program would not run. Ideally, the number of panels per wavelength should be greater than 10. Obviously, output for the lower wavelengths must be considered suspect and subject to considerable discretization error.

Wave Length	Total Number of Panels	Panels per Wavelength
150 m	200	3
300 m	350	12
450 m	500	26

Table 3.1 - Panel Method Discretization

Output from the program gave wave elevations at various positions in front, inside, and behind Deltaport. Figure 3.5 shows the approximate locations of the position markers relative to Deltaport. The exact coordinates are given with the output results. For the purpose of the Panel

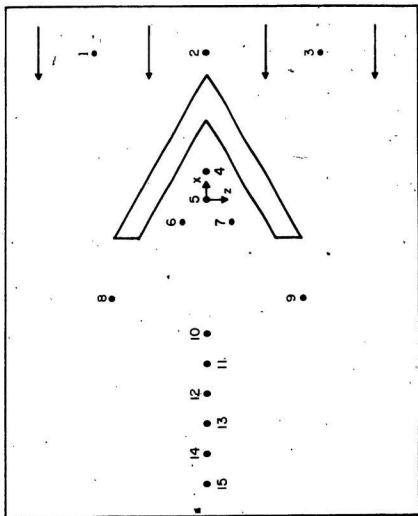


Figure 3.5 Panel Method Position Markers

Method simulation, a non-porous geometry having a rectangular cross-section was assumed. Each leg of the structure was taken to be 600m in length (inside edge) with a draft of 40m. The freeboard is not applicable because the Panel Method is only concerned with the wetted surface area. The width of each leg was simulated to be 90m. Due to the constraints outlined in Section 1.4, the weight of the structure was not needed as input since it is considered to be fixed. It should be noted that the back section of the Deltaport structure was ignored for this computer simulation. The complex sections around the harbour entrance have not been designed to date and are difficult to model with any degree of accuracy.

## EXPERIMENTAL PROGRAM

4.1 Wave Tank Facility

All experimental work for this research was performed in the wave tank laboratory at Memorial University of Newfoundland. This facility is equipped with a piston type wave generator, a towing carriage and a wave attenuating beach. The frequency range for the generator is from 0.3 Hz to 1.3 Hz. The speed range for the towing carriage is from 0.05 m/s to 5 m/s.

The tank has an excellent complement of data acquisition and test equipment.

Figure 4.1 shows a dimensioned detail of the wave tank facility.

4.2 Model Construction

The major objective of the experiment was to isolate and study a two dimensional section of the Deltaport structure. A narrow channel or flume, approximately 0.5 m wide and 5 m long, was first constructed and placed in the wave tank at the position indicated in Figure 4.1. This flume was constructed of wood and galvanized sheet steel. Heavy angle iron was used to structurally reinforce it over its relatively large length to width ratio. It was secured to the bottom using lead weights. It was also braced to the

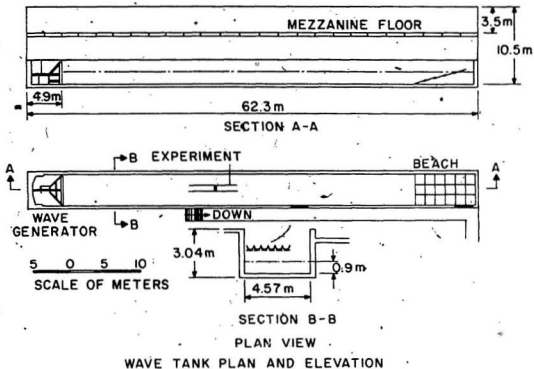


Figure 4.1 Wave Tank Facility

concrete walls of the wave tank to increase its rigidity. Figure 4.2 shows some sketches and pictures of the flume. Holes in its sides, shown in the elevation sketch, were used for barrier support. The pictures show the flume with one of the barriers installed. All of the barriers tested are shown in profile in Figure 4.3. They are described in detail in Section 4.3. Patterns II and IV were chosen to have the approximate depth to width ratio as would the Deltaport. However, it should be noted that the porous pattern shown is not an exact replica of the pattern to be used in the prototype. At present, it would be impossible to model this exactly as the Deltaport is only in a preliminary design phase and the final porosity pattern has not yet been chosen. The flume was placed in the wave tank with the leading edge approximately 18m from the wave generators mid span setting. With the water depth set at 0.9 m, there was approximately 28m from the back end of the flume to the beach at the still water line. The flume was placed forward of the mid tank to ensure that the higher frequency waves generated would remain stable and uniform as they approached the barriers. Care was also taken to avoid reflected waves from the generator. During the 60 second test period employed, reflected waves from the beach did not reach the test site and so were not a problem.

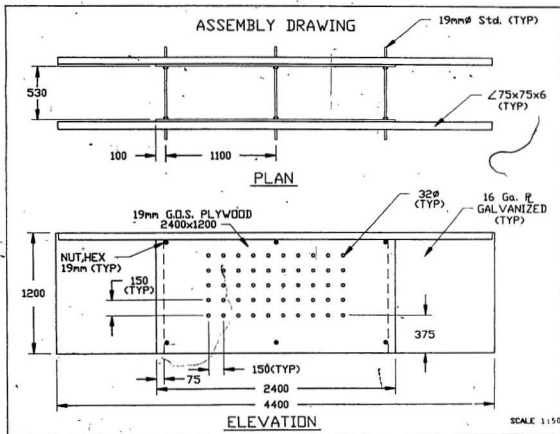
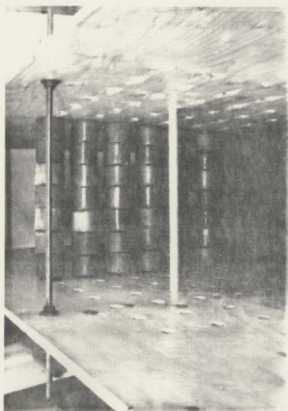
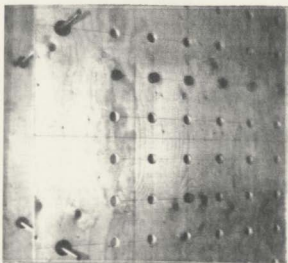


Figure 4.2 Model Construction Drawings and Pictures



Pictures

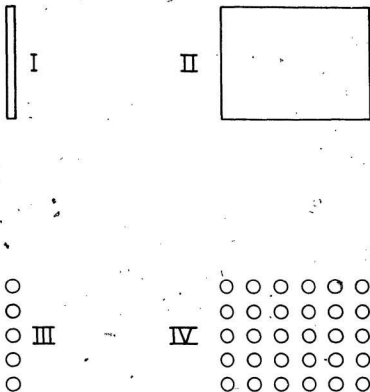


Figure 4.3 Barrier Geometries

#### 4.3 Physical Barriers

As mentioned previously, four barrier geometries were tested in the experiments (Figure 4.3). These were

- I) A solid thin vertical plate
- II) A rectangular or thick vertical configuration
- III) A porous thin plate
- IV) A porous rectangular configuration

The solid thin plate configuration had a depth of 70 cm and a width of 10 cm. It was placed such that it extended approximately 58 cm below the still water line (SWL). It was constructed of 19 mm, good one side (GOS), plywood with only the finished surface exposed to wave action.

The solid thick configuration was similar in construction. Its depth was 70 cm and its width was 85 cm. This depth to width ratio conforms closely to that coming from preliminary Deltaport design and that used in previous model testing [12]. The central section of this configuration was reinforced heavily to negate, as much as possible, any wave energy transference due to flexure of the wooden surfaces.

The overall dimensions of the porous thin plate were basically the same as those of the solid plate. It consisted of a vertical column of cylinders each 10 cm in diameter, spaced such that their centers were 15 cm apart.

Each of the cylinders was fabricated from 10 cm diameter rigid closed cell polystyrene 'cable floats'. Each float had a center bore hole 32 mm in diameter. The floats were press fitted over standard 25 ID / 33.4 OD pipe to give each cylinder its required rigidity. Holes in the sides of the flume were used to support the pipes.

The porous thick configuration had overall dimensions which were basically the same as those of the solid thick geometry. It consisted of 6 vertical columns of cylinders along its width, with horizontal spacing 15 cm center to center. Each column had the porous thin plate layout. This thick configuration was chosen because it resembles the array of the buoyancy tanks coming from preliminary Deltaport design.

Note that the level of porosity in the IIIth and IVth configurations can be adjusted by varying the number of cylinders or the size of the floats. However, only one level was considered in the present exploratory work.

#### 4.4 Model Waves

The characteristics of the waves used to obtain the experimental data were subject to a number of physical and theoretical constraints. For example, limitations on wave height existed due to the size and strength of the model and the accuracy of the wave measuring equipment. The

larger the wave height, the harder it was to control and constrain motions in the model. The smaller the wave height, the less accurate were the measuring probes. Preliminary test work indicated that the ideal range of wave heights would be between 5 cm and 15 cm corresponding to full scale wave heights of 2.5 m and 7.5 m respectively.

Frequencies corresponding to full scale periods of 6 to 10 seconds were chosen for the experiment. At model scale, they were in the range 0.8 Hz to 1.2 Hz.

The chosen wave heights and frequencies were standard wave board settings which match as closely as possible the expected full scale values. It should be noted that only one frequency was generated by the wave board at a given time, creating regular wave forms only.

#### 4.5 . Data Acquisition

The actual experimentation process began with the lowering of the level of the water in the wave tank to 0.9 m. The preconstructed channel shown in Figure 4.2 was then lowered into place in the wave tank and securely fastened to the sides and bottom. At this point, final adjustments were made to the test barrier.

Two sets of experiments were actually conducted. In the first set, a two wave probe procedure was employed to get the reflection coefficient upstream of each geometry

[20]. Unfortunately, the signals from the two probes when processed produced reflection data with enormous scatter and the two probe technique had to be abandoned. In the second set, a single probe was moved through the wave field upstream of each configuration. This gave the wave envelope formed from the superposition of the incident and reflected waves. The reflection coefficient can be obtained directly from this envelope. During the present work, it gave reasonably consistent data with not much scatter. For each test, a total of three resistance type wave probes were installed. The first was set up outside the channel in an area where the incident wave generated by the wave board was unaffected by the set up. Wave probe number two was mounted on the towing carriage in front of the test barrier. The towing carriage, which was set to move at 0.05 m/s, advanced the wave probe through the wave envelope generated by the incident and reflected wave. The data from this probe gave the reflection coefficient R where:

$$R = \frac{H_{\max} - H_{\min}}{H_{\max} + H_{\min}} \quad (4.1)$$

where  $H_{\max}$  is the maximum height of the envelope and  $H_{\min}$  is the minimum height. The third wave probe was also positioned on the towing carriage, but behind the test barrier. This probe directly measured the transmitted wave height. It should be noted, however, that there was no real

necessity for this probe to sweep through the wave field as a stationary probe would have been sufficient. The reason it was mounted on the carriage was simply for the ease of setting it up.

At least once each day before any tests were conducted, the wave generator was used to stir up the water in the tank to ensure consistency in water temperature for the wave probes. After the water had completely settled, each of the three wave probes were individually calibrated.

As the generated wave train advanced into the channel and an approximate steady state was achieved, testing began. Each test had a run time of approximately 60 seconds. During the test, the wave probes in the channel advanced through the wave field. The analog signal from each probe was recorded in three ways:

- 1) The analog signal was directly recorded using a Hewlett Packard 3968A 8-track instrumentation recorder for future analysis.
- 2) The analog signal was sampled and digitized using the Keithley System 570 data acquisition unit and stored on floppy disk for future reference.
- 3) The signal was digitized using the Hewlett Packard 54410A Analog/Digital convertor and viewed on the scope of the Hewlett Packard 5420B digital signal analyzer, simultaneously as the test was being run. This ensured

that all the probes and equipment were functioning properly.

Between each test, the wave tank was allowed to settle for a minimum of 30 minutes.

After the completion of all of the experiments, analysis was performed by feeding the analog signal from the 8-track recorder through the analog/digital converter and into the digital signal analyzer. Software available in this analyzer made the determination of minimum and maximum wave height a relatively straight forward procedure. A cross check of the results was done using the output obtained from the Keithley data acquisition unit. The test results obtained from the above analysis were then recorded on a database for further manipulation and plotting.

#### 4.6 Scale Considerations

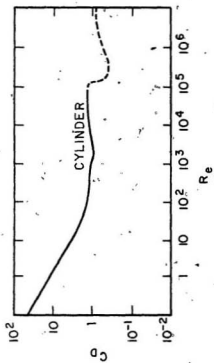
Froude scaling was used to determine the dimensions of the model configuration with respect to the prototype: a scale factor of 1:50 was used. To determine the significance of viscous effects, the Keulegan-Carpenter number was calculated for the model and the prototype. This number is

$$N_{KC} = \frac{VT_p}{D} \quad (4.2)$$

where  $V$  is the flow speed,  $T_p$  is the wave period and  $D$  is

the member diameter. From this number, the viscous drag coefficient can be found [13]. Using a significant wave height of 5 m and wave period of 10 sec for the prototype, the Keulegan-Carpenter number was found to be 4.45. For the experimental configuration, it was calculated to be 4.44. In this range ( $N_{KC} < 5$ ), viscous drag is a significant factor, but according to Sarpkaya [15], the drag coefficient for the model and the prototype would be approximately equal given similar Keulegan-Carpenter numbers.

As a check, the Reynolds number, which was calculated to be approximately  $10^6$  for the model and approximately  $10^7$  for the prototype was plotted on the standard  $C_D$  vs  $Re$  curve [13] shown by Figure 4.4. It was found that the viscous drag coefficient  $C_D$  was approximately the same for both the model and the prototype. Because of this, the errors due to viscous scaling should be negligible.

Figure 4.4  $R_e$  vs  $C_D$

## RESULTS

5.1 Dean's Method

One of the main features of this method is that it assumes 100% of the wave energy is either reflected or transmitted. Figures 5.1 and 5.2 show some R and T predictions generated by this model for a solid thin plate barrier (I in Figure 4.3). As can be seen, as the barrier depth increases, R tends to unity and T tends to zero. Furthermore, this happens faster for the higher frequencies. None of these things are surprising. Note that for a barrier depth of 0.6 m T is down around 10% which implies that only 1% of the incident wave energy gets past the barrier. Recall that at the model scale the prototype depth is around 0.6 m. Thus, if the Deltaport structure was nonporous and diffraction was not important, then there should be insignificant wave action within its harbor.

5.2 The SOLA-VOF Method

Figures 5.3 and 5.4 show some results from the SOLA-VOF simulation. Here and throughout, calculated points have been joined by straight lines. For the simulation, the barrier was rectangular and had zero porosity (II in Figure 4.3). Seventeen columns of cells, each cell 5 cm on a side, were used to construct the barrier. As can be seen, even

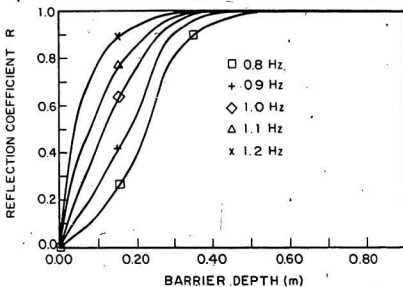


Figure 5.1 Reflection vs Barrier Depth: Dean's Method

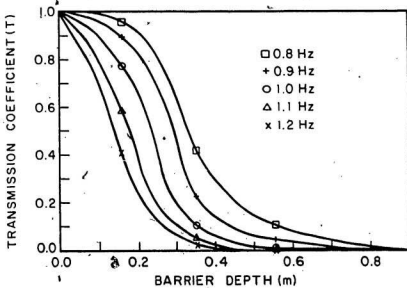


Figure 5.2 Transmission vs Barrier Depth: Dean's Method

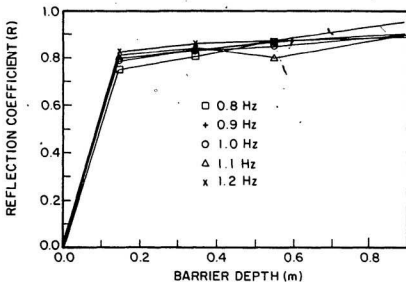


Figure 5.3 Reflection vs Barrier Depth: SOLA-VOF

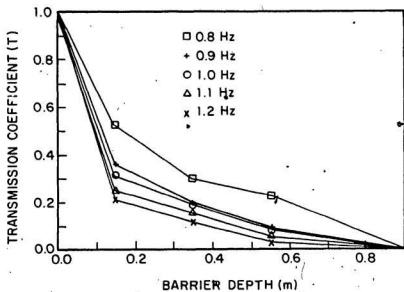


Figure 5.4 Transmission vs Barrier Depth: SOLA-VOF

though the barrier is thicker, the trends for R and T are in agreement with Dean's analysis. Recall that in SOLA-VOF the prototype water depth can be modelled. However, for the operating frequencies, the waves generated do not feel the bottom. So, the water is effectively deep.

If there was no dissipation and the waves were steady and not contaminated by parasitic phenomena, then all of the energy should ideally be accounted for in reflection and transmission. Here, an average of 85% of the incident wave energy was accounted for by SOLA-VOF, and all of the runs fell in the range of 80.3% to 90.1%. We feel that the majority of this energy imbalance is due to computer discretization error. However, transient and parasitic wave phenomena may also be important. Unfortunately, they are hard to quantify. They would introduce errors in the envelope as well as in the incident and transmitted waves. Viscosity and surface tension may also contribute to the imbalance. The following two sections briefly study these phenomena.

#### 5.2.1 Viscosity Effects

For several runs, the fluid viscosity was set to zero. Table 5.1 shows some comparisons of those runs with runs which had viscosity set equal to the laminar viscosity of water.

Freq.	Barrier Depth	$\mu=0$		$\mu=0$	
		R	T	R	T
0.8	.15	.754	.524	.775	.585
1.0	.35	.836	.190	.848	.200
1.2	.55	.955	.030	.962	.045

Table 5.1 - SOLA-VOF: Viscous Effects

From the results, it can be seen that viscosity on average accounts for only 2.4% of the total energy and so for solid barriers its effect is insignificant. This is really not surprising because the corners of the barrier, where viscous phenomena should dominate, are at a depth where there is very little water motion. As expected, there is less transmission with the inclusion of viscosity. Note that a false diffusion is inherent in the upwind treatment of the convective terms in the governing equations; especially when the grids are coarse and the flows are high speed. This has a dissipative or viscous-like effect on wave energy. It is probably partly responsible for the energy imbalances noted throughout.

### 5.2.2 Surface Tension Effects

Most program runs were conducted with zero surface tension. As a check on the accuracy of this assumption, several runs were performed using the normal surface tension for an air-water interface. Results from these checks are outlined in Table 5.2

Freq.	Barrier Depth	$\sigma = 0$		$\sigma \neq 0$	
		R	T	R	T
0.8	.15	.754	.524	.786	.590
1.0	.35	.836	.190	.865	.200
1.2	.55	.955	.030	.972	.040

Table 5.2 - SOLA-VOF: Surface Tension Effects

From the results, it can be seen that surface tension on average accounts for only 3.8% of the total energy and so its effect is insignificant. Because of the wavelengths and the size of the solid barrier tested, this is not surprising. On the other hand, surface tension may be important for porous configurations if the tubes are

small and closely spaced. However, it should be noted that the CPU time required for execution is approximately 3.5 times greater when surface tension is included.

### 5.2.3 Effect of Grid Size

To check the effect of changing the grid size on the accuracy of the results, the number of divisions on the x and y axis were doubled, thus reducing the area of the cell size to 1/4 of the original. The check was done using a frequency of 1.0 Hz and a barrier depth of 35 cm. The effect of reducing the grid size was to increase the amount of energy accounted for from 85% to 95%, and so it increases computational accuracy. Unfortunately, the reduction in cell size increased the computer CPU time required for the calculations from 3.5 hours to 27 hours. So, the runs become computationally expensive. We felt it was unnecessary to redo this run and all of the previous runs with an even more refined grid because the Deltaport design is still in the preliminary stage. We do not need extremely accurate results at this stage. What we have shown above is that, once the design is finalized, we do have a procedure that can accurately predict performance.

### 5.3 Comparisons of SOLA-VOF and Dean's Method

Results from SOLA-VOF and Dean's method are shown

together in Figures 5.5 through 5.9 inclusive. For the SOLA-VOF runs, the barrier was thin and had zero porosity (I in Figure 4.3). One column of cells was used to create it in the grid. All plots show a general agreement in trends and if the positive difference between all five data points on each plot are compared one against the other, then the average variance of all the comparisons computes to be approximately 10%. Obviously, most of this discrepancy is due to discretization error.

#### 5.4 The Panel Method

The Panel Method places the Deltaport configuration in a three dimensional wave field. The triangular shape of the Deltaport structure produces some complex wave patterns both in front and behind the structure.

Typical output data are shown in Table 5.3. In this table, all wave heights are relative to an incident wave height of 1. The influence of the reflected wave can easily be seen in positions 1 through 3 which are fixed and located in front of the structure. The complex wave envelope, as generated, produces nodes and peaks at different points on the ocean surface for different wave lengths.

Pos. No.	Position Coordinates		Wave Height (m)		
	X	Z	$\lambda=150m$	$\lambda=300m$	$\lambda=450m$
1	500	-370	0.842	0.615	1.013
2	500	0	0.731	1.803	0.899
3	500	370	0.842	0.615	1.013
4	100	0	0.418	0.161	0.652
5	0	0	0.257	0.225	0.422
6	-50	-75	0.357	0.609	0.519
7	-50	75	0.357	0.609	0.519
8	-300	-370	1.059	1.580	1.083
9	-300	370	1.059	1.580	1.083
10	-500	0	0.257	0.305	0.803
11	-700	0	0.296	0.262	0.857
12	-900	0	0.385	0.300	0.874
13	-1100	0	0.455	0.354	0.882
14	-1500	0	0.548	0.446	0.889
15	-2000	0	0.653	0.855	0.895

Table 5.3 - Panel Method Program Results

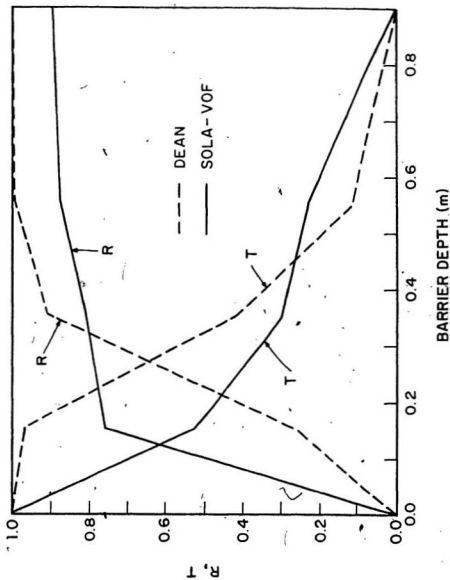


Figure 5.5 Dean's Method vs SOLA-VOF: 0.8 Hz

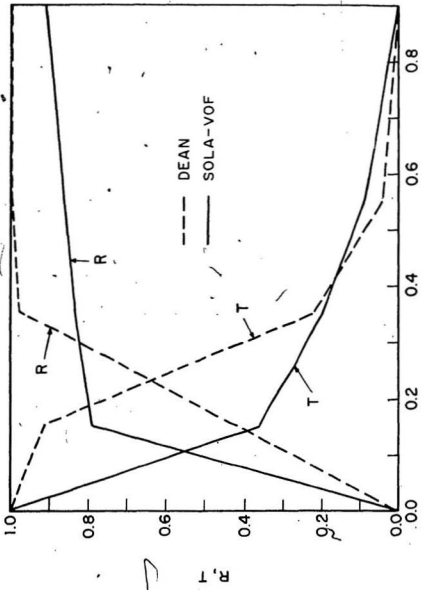


Figure 5.6 Dean's Method vs SOLA-VOF: 0.9 Hz

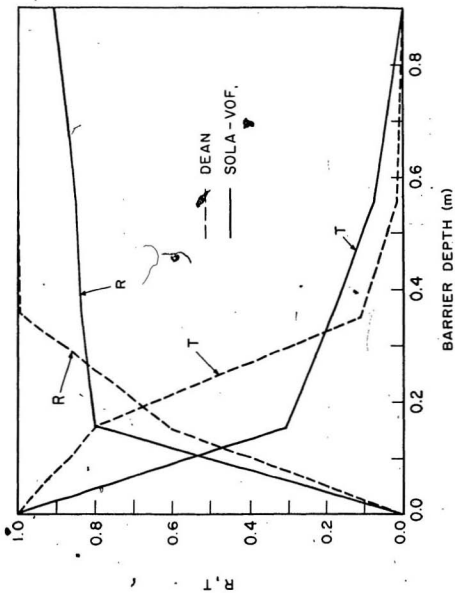


Figure 5.7 Dean's Method vs SOLA-VOF: 1.0 Hz

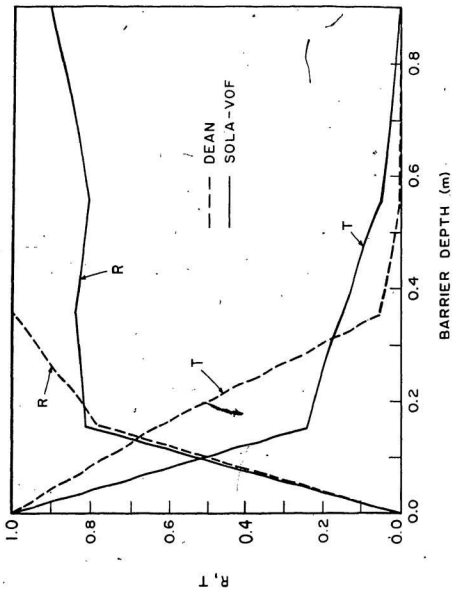


Figure 5.8  
Dean's Method vs SOLA-VOF: 1.1 Hz

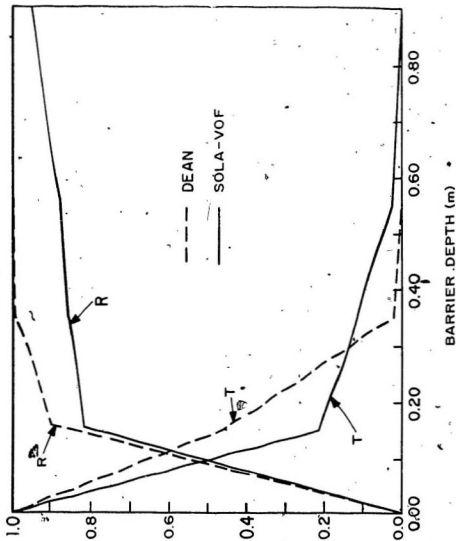


Figure 5.9 Dean's Method vs SOLA-VOF: 1.2 Hz

In the area behind the structure where a reduced wave height is desired, there is also a complex scattered wave field which produces some interesting results. Positions 4 through 7, which are fixed and located to the rear but enclosed by the main structure, all have wave heights which are reduced significantly. The inconsistency of the results is due to the fact that there is a complex three dimensional wave field with multiple reflections present in this area.

Position markers 8 and 9 are located behind the Deltaport structure, but on the extreme left and right edges where a heavy influence from the incident wave diffracting around the corner can be expected. All wave lengths generated show this pattern.

Position markers 10 through 15 are all located behind the structure and on the x axis center line. Far behind, one would expect the wave height to tend back to 1. The transmitted wave heights for positions 10 through 15 clearly show this pattern. The average wave heights behind the structure are:

$$\lambda = 150 \text{ m} \quad .508$$

$$\lambda = 300 \text{ m} \quad + \quad .609$$

$$\lambda = 450 \text{ m} \quad + \quad .790$$

This also matches the hypothesis which states that, as the wave length increases, the transmitted wave height increases.

The Shore Protection Manual published by the US Army Coastal Engineering Research Center [1] gives diffraction patterns beyond a fixed structure as waves from a given direction impinge on it. The structure is considered to be a semi infinite fixed breakwater which, for the purposes of simple comparison, can be modelled as one leg of the Deltaport structure. Figure 5.10 gives the pattern corresponding to Deltaport. Table 5.4 gives a Panel Method/ Shore Protection Manual comparison.  $K = H/H_t$  is the Shore Protection Manual diffraction parameter.

Waveheights in the harbor region from the Panel Method analysis computed to be slightly higher than those calculated from the Shore Protection Manual. This makes sense as extra energy can get into the harbor by passing beneath, through and diffracting around two corners of the Deltaport.

Well outside the harbor region, Panel Method values of waveheight are lower than those calculated from the Shore Protection Manual. This could be due to a finite water depth effect or to computer discretization error in the Panel Method program. Table 3-1 indicates this discretization might be a problem at lower wavelengths. In fact, the error between the values from the two methods is found to be higher at lower wavelengths which is consistent

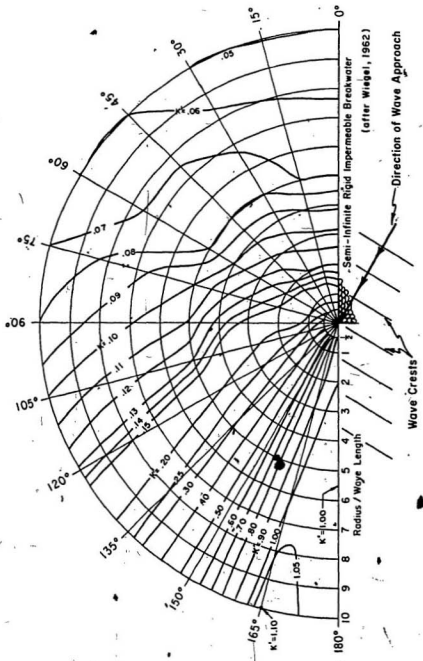


Figure 5.10 Wave Pattern from Shore Protection Manual

Pos.	$\lambda = 150 \text{ m}$		$\lambda = 300 \text{ m}$		$\lambda = 450 \text{ m}$	
	K	Panel Method	K	Panel Method	K	Panel Method
5	.135	.257	.180	.225	.230	.422
7	.156	.357	.230	.609	.275	.519
9	1.000	1.059	1.000	1.580	1.000	1.083
10	.630	.257	.650	.305	.700	.803
11	.880	.296	.820	.262	.810	.857
12	.980	.385	.850	.300	.820	.874
13	1.000	.455	.990	.354	.900	.882
14	1.000	.548	1.000	.446	.950	.889
15	1.000	.653	1.000	.855	1.000	.895

Table 5.4 Panel Method/Shore Protection Manual Comparison

with this hypothesis. This effect was also confirmed by Sarpkaya and Isaacson [13].

Although there were some discrepancies between the Panel Method and the data from the Shore Protection Manual, results were encouraging. The trends were very similar and the results tended to converge as the wavelength increased.

## 5.5 Experiment

### 5.5.1 Thin Plate Case

Figure 5.11 gives R and T results for the solid thin plate (I in Figure 4.3). Figure 5.12 gives results for the porous thin plate (III in Figure 4.3) which had 33% of its frontal area open to wave action. As can be seen, porosity decreases R and increases T. This is not really surprising.

### 5.5.2 Rectangular Barrier Case

For the porous rectangular configuration, the cylinder spacing produced a barrier which was 60% vacant space. Figure 5.13 gives the solid barrier results (II in Figure 4.3), and Figure 5.14 gives the porous barrier results (IV in Figure 4.3). As can be seen, the trends with respect to R and T resemble the thin plate trends. Also, thicker barriers generally have less transmission, which is really not surprising especially for the porous configurations.

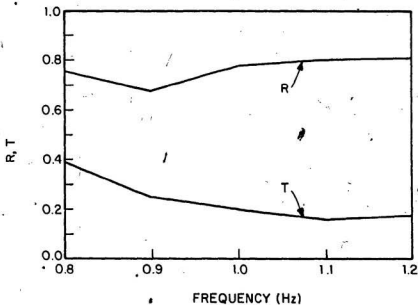


Figure 5.11 Experimental Data: Solid Thin Plate

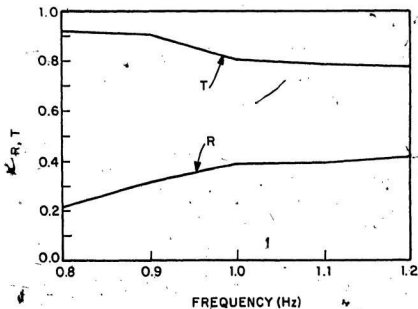


Figure 5.12 Experimental Data: Porous Thin Plate

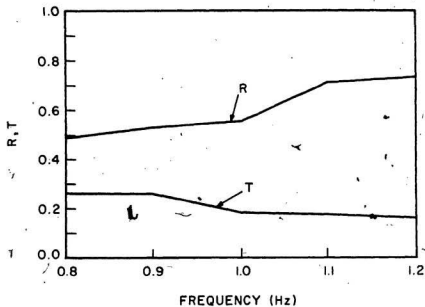


Figure 5.13 Experimental Data: Solid Rectangular Barrier

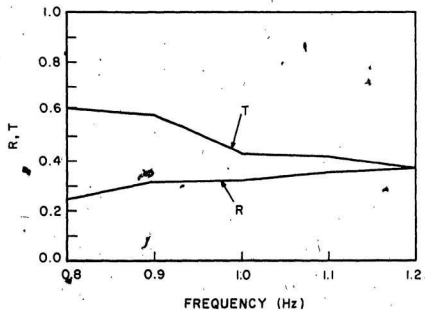


Figure 5.14 Experimental Data: Porous Rectangular Barrier

### 5.6 Comparisons of SOLA-VOF and the Thin Plate Experiments

The SOLA-VOF program was run to match the set up of the thin plate experiments. A comparison of the results for a non-porous configuration is given in Figure 5.15. There is reasonable agreement with an average variance of approximately 10%.

For a thin plate barrier having a porosity level of 33%, SOLA-VOF, with the grid shown in Figure 5.16, gave for frequency  $f = 1$  hz,  $R = 0.64$  and  $T = 0.39$ , while the experiment gave  $R = 0.32$  and  $T = 0.42$ . Obviously, SOLA-VOF, with such a coarse grid, suffers from considerable discretization error. Nevertheless, the results are encouraging. In general, the waves were steeper in the experiments than in the simulation. In fact, wave steepness was something difficult to set. It may have been a factor in the discrepancies noted here and elsewhere. For the corresponding rigid case, SOLA-VOF gave  $R = 0.85$  and  $T = 0.09$ . It should be noted that only one porous case was run due to the extreme amount of CPU time required to obtain a solution. The case given here ran for more than five days on the VAX 8800 (LEIF) system at MUN. To do more runs was deemed to be very inconsiderate of other students wanting to run routine programs. Also, the probability for the computer to experience downtime in a five day period is very high and several runs terminated due to this fact.

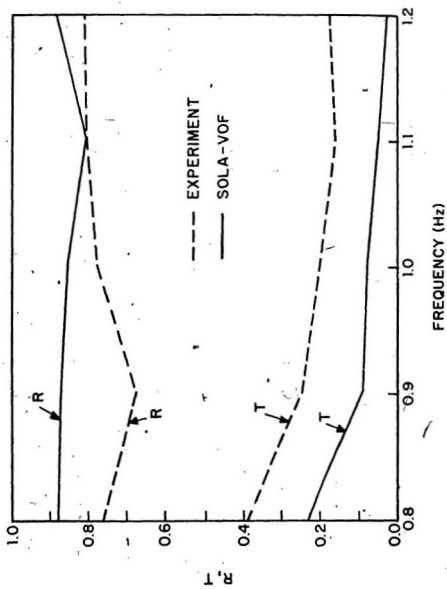


Figure 5.15 Experimental/SOLA-VOF Comparison

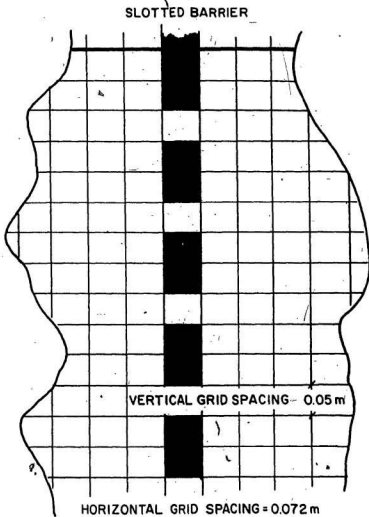


Figure 5.16 Porous Barrier Geometry: SOLA-VOP

## CONCLUSIONS AND SUGGESTIONS FOR FUTURE WORK

The wave attenuation characteristics of the Deltaport floating breakwater were studied theoretically and experimentally. Two of the theoretical procedures assumed a two dimensional geometry. One was based on potential flow concepts (Dean's Method) and the other was based on the Navier-Stokes equations (SOLA-VOF). An important feature of the latter is it can handle the porous nature of the breakwater. A three dimensional potential flow procedure known as the Panel Method was also used to study the Deltaport performance. It assumed the structure to be nonporous. For the experiments, a two dimensional section of the Deltaport structure was tested in the wave tank at Memorial University.

The following conclusions were reached:

- 1) For the two dimensional section of the Deltaport structure, the SOLA-VOF Method and the experimental data show reasonable agreement. The agreement is best when porosity is low. Unfortunately, the SOLA-VOF Method is computationally very expensive. Because of this, the grids used for the present work were quite coarse and the results contain significant discretization errors. Local refinement of the grid near the barriers, with coarser grids used elsewhere, might help with this.

- 2) When porosity is low, Dean's Method and the SOLA-VOF Method show reasonable agreement. Unlike the SOLA-VOF Method, Dean's Method is computationally inexpensive. So, it can be used to get a rough but quick look at breakwater performance when porosity is low.
- 3) When porosity is low, the Panel Method can be used to study the attenuation characteristics of the three dimensional Deltaport structure. It produces results which are qualitatively in agreement with diffraction patterns taken from the Shore Protection Manual.

Some suggestions for future work are:

- 1) The SOLA-VOF program in its present form would require a very fine grid to deal with turbulent flow within the breakwater structure. This is because the scale of turbulence is very small. The program could be improved in this regard with the addition of a two equation turbulence model such as the  $k-\epsilon$  model developed at Imperial College [10]. This model accounts for the convection, diffusion, production and dissipation of turbulence and does not require a fine grid. Such a model should be added to the SOLA-VOF code and the new code should then be used to study various porosity levels and patterns.

- 2) An attempt should be made to add porosity to the Panel Method code. This could be based on the porous-plug or Darcy flow model for waves propagating over a porous seabed. A quasi-steady hydraulic resistance model for the structure might also work. If neither of these things work, an attempt should then be made to develop corrections for the Panel Method based on the two dimensional setup. Attenuation due to the back section of the Deltaport should also be examined with the code.
  - 3) When the breakwater structure is more defined, a large two dimensional section of it should be installed and tested in the wave tank at the Institute for Marine Dynamics (IMD).
  - 4) Steep wave phenomena should be studied both theoretically (SOLA-VOF) and experimentally (IMD).
- JR

REFERENCES

1. Shore Protection Manual (1985), U.S. Army Corps of Engineers.
2. Seelig, W.N. (1980): "Two Dimensional Tests of Wave Transmission and Reflection Characteristics of Laboratory Breakwaters", U.S. Army Corps of Engineers, Virginia, June.
3. Snyder, G., Murray, J.J. and Muggeridge, D.B. (1980): "Design and Testing of a Tethered Float Breakwater"; Memorial University of Newfoundland, St. John's.
4. Tokuo, Y.M. and Akinori, Y. (1979): "Large Wave Tank Tests on Taut-Moored Breakwaters", Proceedings of the Conference on Coastal Structures, pp. 1067-1105.
5. Kowlaski, T. (ed) (1974): "Floating Breakwaters Conference Papers", University of Rhode Island, Rhode Island; U.S.A., pp. 1-112, 181-191, 213-232, 247-261.
6. Lee, J.J. and Walther, J.A. (1974): "Wave Energy Permeation of San Pedro Breakwater"; Proceedings of the Offshore Technology Conference, Dallas, U.S.A.
7. Murakami, H., Hosoi, Y. and Goda Y. (1987): "Analysis of Permeable Breakwaters", Proceedings of the 20th International Coastal Engineering Conference, Taipei, Taiwan.
8. Madsen, O.S. (1974): "Wave Transmission Through Porous Structures", Proceedings of the ASCE Journal Waterways, Harbors and Coastal Engineering Division, Vol. 100, No. WW3.
9. Finnigan, T.D. and Yamamoto, T. (1979): "Analysis of Semisubmerged Porous Breakwaters", Proceedings of the Fourth Conference on Civil Engineering in the Ocean, San Francisco (ASCE).
10. Gosman, A. and Ideriah, F. (1976): "Teach-T: A General Computer Program for Two-Dimensional Turbulent Recirculating Flows", Imperial College of Science and Technology, London, Department of Mechanical Engineering Report.

11. Billard, D. (1984): "An Economic Analysis of the Deltaport Concept", Memorial University of Newfoundland, St. John's, Newfoundland.
12. Cheema, S. and Nolan, C. (1985): "Initial Testing Performed on the 1:200 Scale Deltaport Model", Memorial University of Newfoundland, St. John's, Newfoundland.
13. Sarpkaya, T. and Isaacson, M. (1981): "Mechanics of Wave Forces on Offshore Structures", Van Nostrand Reinhold, New York, pp. 150-156.
14. Dean, R. and Dalrymple, R. (1984): "Water Wave Mechanics for Engineers and Scientists", Section 9.4, Prentice-Hall, Englewood Cliffs, New Jersey.
15. Sarpkaya, T. "Wave Loading in the Drag/Inertia Regime with Particular Reference to Groups of Cylinders", Naval Postgraduate School, Monterey, California, USA.
16. Dean, W.R. (1945): "On the Reflection of Surface Waves by a Submerged Plane Barrier", Proceedings of the Cambridge Philosophical Society, vol. 41, pp. 231-238.
17. Wehausen, J.V. and Laitone, E.V. (1960): "Encyclopedia of Physics", Springer-Verlag, Berlin, Germany, vol. 9, pp. 526-533.
18. Nichols, B.D., Hirt, C.W., Hotchkiss, R.S. (1980): "SOLA-VOF: A Solution Algorithm for Transient Fluid Flow with Multiple Free Boundaries", Los Alamos Scientific Laboratory, Los Alamos, New Mexico, U.S.A.
19. Sen, D. (1983): "Prediction of Wave Loads and Motions of Floating Marine Structures by Three Dimensional Wave-Flow Theory", Memorial University of Newfoundland, St. John's, November.
20. Goda, Y. and Suzuki, Y. (1976): "Estimation of Incident and Reflected Waves in Random Wave Experiments", Ministry of Transport-Marine Hydrodynamics Division, Japan, pp. 828-830.







